Version of Record: https://www.sciencedirect.com/science/article/pii/S1567576921001235
Manuscript_d0d15b036c97c989607ea18fd9d1c570

Running title Role of Cateslytin in Cardiomyocytes

Cateslytin abrogates lipopolysaccharide-induced cardiomyocyte injury by reducing inflammation and oxidative stress through toll like receptor 4 interaction

Carmine Rocca[#1], Anna De Bartolo[#1,2], Fedora Grande[3], Bruno Rizzuti[4], Teresa Pasqua[1,5], Francesca Giordano[2], Maria Concetta Granieri[1], Maria Antonietta Occhiuzzi[3], Antonio Garofalo[3], Nicola Amodio[6], Maria Carmela Cerra[7], Francis Schneider[8,9], Maria Luisa Panno[2], Marie Hélène Metz-Boutigue[9,10*] & Tommaso Angelone[1,11*]

[1] Laboratory of Cellular and Molecular Cardiovascular Pathophysiology, Department of Biology, E and E.S., University of Calabria, Rende, CS, Italy.

[2] Department of Pharmacy, Health and Nutritional Sciences, University of Calabria, Rende, CS, Italy.

[3] Laboratory of Medicinal and Analytical Chemistry, Department of Pharmacy, Health and Nutritional Sciences, University of Calabria, Rende, Italy.

[4] CNR-NANOTEC, Licryl-UOS Cosenza and CEMIF.Cal, Department of Physics, University of Calabria, Rende, Italy.

[5] Department of Health Science, University of Catanzaro Magna Graecia, 88100 Catanzaro, Italy.

[6] Department of Experimental and Clinical Medicine, Magna Graecia University of Catanzaro, Catanzaro, Italy.

[7] Laboratory of Organ and System Physiology, Department of Biology, E and E.S., University of Calabria, Rende, CS, Italy.

[8] Department of Intensive Care, Hospital Hautepierre, University of Strasbourg, Strasbourg, France.

[9] Inserm UMR 1121, Fédération de Médecine Translationnelle, University of Strasbourg, Strasbourg, France.

[10] Faculty of Odontology, University of Strasbourg, Strasbourg France.

[11] National Institute of Cardiovascular Research (INRC), Bologna, Italy.

# These authors equally contributed to this work

Corresponding Authors

* Prof. Tommaso Angelone, University of Calabria, 87036 Arcavacata di Rende (CS), Italy. E-mail: tommaso.angelone@unical.it

* Dr. Marie Hélène Metz-Boutigue, University of Strasbourg, Strasbourg, France. E-mail: marie-helene.metz@inserm.fr

© 2021 published by Elsevier. This manuscript is made available under the CC BY NC user license
https://creativecommons.org/licenses/by-nc/4.0/

Abstract

Global public health is threatened by new pathogens, antimicrobial resistant microorganisms and a rapid decline of conventional antimicrobials efficacy. Thus, numerous medical procedures become life-threating. Sepsis can lead to tissue damage such as myocardium inflammation, associated with reduction of contractility and diastolic dysfunction, which may cause death. In this perspective, growing interest and attention are paid on host defence peptides considered as new potential antimicrobials. In the present study, we investigated the physiological and biochemical properties of Cateslytin (Ctl), an endogenous antimicrobial chromogranin A-derived peptide, in H9c2 cardiomyocytes exposed to lipopolysaccharide (LPS) infection. We showed that both Ctl (*L* and *D*) enantiomers, but not their scrambled counterparts, significantly increased cardiomyocytes viability following LPS, even if *L*-Ctl was effective at lower concentration (1 nM) compared to *D*-Ctl (10 nM). *L*-Ctl mitigated LPS-induced LDH release and oxidative stress, as visible by a reduction of MDA and protein carbonyl groups content, and by an increase of SOD activity. Molecular docking simulations strongly suggested that *L*-Ctl modulates TLR4 through a direct binding to the partner protein MD-2. Molecular analyses indicated that the protection mediated by *L*-Ctl against LPS-evoked sepsis targeted the TLR4/ERK/JNK/p38-MAPK pathway, regulating NFkB p65, NFkB p52 and COX2 expression and repressing the mRNA expression levels of the LPS-induced proinflammatory factors IL-1β, IL-6, TNF-α and iNOS. These findings indicate that Ctl could be considered as a possible candidate for the development of new antimicrobials strategies in the treatment of myocarditis. Interestingly, *L*-enantiomeric Ctl showed remarkable properties in strengthening the anti-inflammatory and anti-oxidant effects on cardiomyocytes.

Keywords

Cardiomyocytes, Cateslytin, Antimicrobial Peptides, Inflammation, Oxidative Stress, Toll-like receptor 4

1. Introduction

Evidences from epidemiological studies conducted on post-mortem individuals identified myocarditis as a significant cause of unexpected death, representing a major reason of cardiovascular events. Myocarditis is a potentially life-threatening disease and mostly occurs in young and adult people [1]. Accordingly, biopsy-proven myocarditis was reported in 9–16% of adult patients and a prevalence of myocarditis of 2-42% of cases in young people was registered [1 and references therein]. Several viral and bacterial infections represent etiological agents of myocarditis. Among them, the severe acute respiratory syndrome coronavirus 2 (SARS-CoV-2) can cause myocarditis as evinced by numerous recent investigations reporting cases of acute myocarditis or myocardial inflammation in coronavirus disease 2019 (COVID-19) [2,3 and references therein]. Also, direct infection of the heart muscle by bacteria and bacteria-produced toxins can be responsible of myocarditis and severe myocardial damage. Bacterial myocarditis is usually observed in the context of a severe sepsis, such as an infection induced by Gram-negative bacteria, that can lead to multi-organ failure, including heart dysfunction and arrhythmias that can occur in around 60% of septic patients [4]. Clinical and experimental studies have extensively reported how decreased contractility and impaired myocardial compliance constitute major factors causing myocardial dysfunction in sepsis [5].

Lipopolysaccharide (LPS) represents the major component of the outer membrane of Gram-negative bacteria that belongs to the pathogen-associated molecular patterns (PAMPs). During myocardial inflammation, LPS interacts with the key member of pattern-recognition receptors (TLRs), the toll-like receptor 4 (TLR4), expressed on the surface of host cardiomyocyte, stimulating the innate immune system and inducing the inflammatory response [6]. TLR4 activation by LPS induces the myeloid differentiation factor 88 (Myd88)-dependent pathway, converging on nuclear transcription factors activation, such as nuclear factor-kB (NFkB). This, in turn, induces the production of pro-inflammatory cytokines leading to inflammatory cascades that are associated with several cardiovascular diseases, including myocarditis and heart failure [7 and references therein].

The identification of new classes of drugs to include in the therapeutic options for inflammatory dilated cardiomyopathy and myocarditis, for which the availability of specific treatment remains limited, is of crucial clinical interest. This is particularly important also given the global increasing impact of antibiotic-resistant infections on health and economic outcomes [8]. In this context, antimicrobial peptides (AMPs) are antimicrobial agents active against infections that do not show the typical disadvantages of more conventional antibiotics related to possible gastrointestinal or allergic reactions, and associated to antibiotic-resistant bacteria [9].

Chromogranin A (CgA), a member of the chromogranin/secretogranin family, is a pro-hormone localized in the secretory vesicles of neurons, neuroendocrine cells, granulocytes, immune cells and cardiomyocytes [10-12]The intravesicular proteolytic processing of CgA under physiological or stress conditions generates several protein fragments with different biological activities [12], ranging from the regulation of innate immunity, antimicrobial activities and inflammation to neuroprotection and cardiovascular protection

[13,14,15]. One of the CgA cleavage products, the bioactive peptide Catestatin (Cst, human $CgA_{352–372}$) was initially described as a potent inhibitor of catecholamines release via the nicotinic receptor [16]. Experimental evidences report that Cst may affect the heart function and the blood pressure both directly and indirectly, playing a crucial regulatory role in cardiovascular system under physiological and pathological conditions [13,17]. Accordingly, Cst is able to counteract the cardiac effects following adrenergic stimulation, and to protect the heart against ischemia/reperfusion injury, acting as a post-conditioning protective agent [13]. It is also known that Cst contributes to the immune system regulation and can mitigate severe inflammatory response, thus preserving tissues function [17].

In addition to several other AMPs resulting from the natural processing of CgA, such as vasostatin-1, the core sequence of Cst, Cateslytin (Ctl; bovine $CgA_{344–358}$, with sequence RSMRLSFRARGYGFR), can also act as host defense peptides (HDPs), due to its antimicrobial activities against a wide number of pathogens [18]. In addition, compared to other CgA fragments with antimicrobial properties, Ctl is able to resist to the degradation when treated with bacterial supernatants [19] and it is unable to induce resistance for the host [20].

Based on these knowledges, the present work was undertaken to explore: i) the ability of the two enantiomers of the Ctl (*L* or *D* amino acids) to mitigate the cardiomyocyte injury evoked by LPS infection; ii) the potential ability of *L*-Ctl to affect TLR4 through interaction with the partner protein MD-2; iii) the molecular mechanism of action underlying the effect of *L*-Ctl in the presence of LPS in H9c2 cardiomyocytes.

2. Material & Methods

2.1. Peptides and chemicals

L-Ctl ($CgA_{344–358}$, RSMRLSFRARGYGFR) and its derivate *D*-Ctl were synthesized by Proteogenix SAS (Schiltigheim, France) according to the Merrifield Technique, a stepwise solid-phase peptide synthesis approach with FMOC chemistry, and purified to >95% by using reverse phase high-performance liquid chromatography (RP-HPLC) and controlled by MALDI-TOF mass spectrometry. As negative controls, the scrambled *L*-Ctl and *D*-Ctl (FMRLRYRSSAFGGRR, in *L*-and *D*-aminoacid forms, respectively) have been used. Both *L*-Ctl and *D*-Ctl were dissolved in sterile water before use (UltraPure RNase/DNase-free distilled water, Invitrogen, California, USA). Lipopolysaccharides (LPS) from *Escherichia coli* O55:B5, sodium pyruvate and β-nicotinamideadenine dinucleotide disodium salt, 2,4 dinitrophenylhydrazine (DNPH), 2-thiobarbituric acid (TBA), bovine serum albumin (BSA), butanol-1, butylated hydroxyanisole, diethyl ether, ethylenediaminetetraacetic acid (disodium salt), streptomycin sulfate, tween-20 and urea were obtained from Sigma Aldrich (St. Louis, MO, USA). Dimethyl sulfoxide (DMSO) was purchased from PanReac AppliChem (Glenview, Illinois, USA). Absolute ethanol, ethyl acetate, hydrochloric acid, methanol and trichloroacetic acid were purchased from Carlo Erba Reagents (Cornaredo, MI, Italy).

2.2. Cell culture

H9c2 cells (rat embryonic cardiomyocytes) were obtained from American Type Culture Collection (ATCC, Manassas, VA, USA) (Cat# CRL-1446_H9c2, RRID:CVCL_0286) and maintained in Dulbecco's Modified Eagle Medium/Nutrient Mixture F-12 (DMEM/F-12, Gibco, Thermo Fisher Scientific, Waltham, MA, USA) containing 10% fetal bovine serum (FBS, Gibco) and supplemented with 1% penicillin/streptomycin (Thermo Fisher Scientific), incubated at 37°C in humidified atmosphere with 5% CO_2 [21]. When the cells reached a density of 80% in 100-mm dishes, they were digested using 0.25% Trypsin-EDTA (1X) (Gibco) according to a 1:2 ratio following manufacturer's instructions (ATCC). For each experiment, the cells were seeded and incubated for 48 h at 37°C, 95% O_2 and 5% CO_2.

2.2.1. Cell viability assay

H9c2 cell viability was evaluated by 3-(4,5-dimethylthiazol-)2,5-diphenyl tetrazonium bromide (MTT) assay, as previously described [21]. The cells were seeded at a density of 5×10^3 cells/well in 96-well plate and exposed to the following treatments: Control (vehicle), *L*-Ctl (from 1 to 100 nM), *D*-Ctl (from 1 to 100 nM), LPS (10 µg/mL) alone, LPS + *L*-Ctl (from 1 to 100 nM), LPS + *D*-Ctl (from 1 to 100 nM), LPS + scrambled *L*-Ctl (from 1 to 100 nM) and scrambled *L*-Ctl (from 1 to 100 nM) for 6 h [22]. The control was treated with the vehicle (UltraPure RNase/DNase-free distilled water). At the end of the treatments, the cell culture medium was replaced with 100 µl of 2 mg/ml MTT solution (Sigma Aldrich) and the cells were incubated for 4 h at 37°C, 5% CO_2. After incubation, the solution was removed and the formazan crystals were solubilized by adding 100 µl of DMSO for 30 min. The absorbance was measured using a Multiskan EX Microplate Reader Lab (Thermo Fisher Scientific) at 570 nm. The means of absorbance values of six wells in each experimental group were expressed as the percentage of cell viability. The experiment was repeated three independent times. Cell viability were reported as percentage of cells survival relative to control cells.

2.2.2. Biochemical analyses of H9c2 cells

2.2.2.1. Lactate dehydrogenase (LDH) activity determination

The structural integrity of cultured H9c2 cardiomyocytes was evaluated by determining the level of LDH released in the culture supernatant. To this aim, the cells were seeded in a 24-well plate at a density of 1×10^5 cell/ml and treated with vehicle (control), LPS (10 µg/mL), LPS + *L*-Ctl (1 nM) and *L*-Ctl (1 nM) alone for 24 h. 100 µl of the culture supernatant per well was used for LDH activity determination. The enzyme activity was evaluated spectrophotometrically (GENESYS 20 spectrophotometer, Thermo Fisher Scientific), following the method of McQueen (1972) [23]. After incubation of reagents, absorbance at 340 nm was recorded every min until steady-state was reached. The reaction velocity was determined by a decrease in

absorbance at 340 nm, resulting from the oxidation of NADH indicative of LDH activity, that was expressed in IU/L [24].

2.2.2.2. Evaluation of malondialdehyde (MDA) concentration

The concentration of MDA (as an indicator of lipid peroxidation following ROS generation) in H9c2 cell lysates was determined by thiobarbituric acid reactive substances (TBARS) assay, as previously described [25-27]. The cells were seeded in a 24-well plate at a density of 1×10^5 cell/ml and treated as described above for 6 h. Subsequently, cells were washed with cold phosphate buffered saline (PBS), centrifuged at 300 × g for 10 min and the supernatant was removed. The precipitate obtained was resuspended in 1 mL of a cold sodium phosphate buffer 10 mM (containing 1 mM ethylenediaminetetraacetic acid and 1 mM butylated hydroxyanisole in 0.15 % ethanol), pH = 7.2 and crushed by ultrasonic wave. MDA concentration was estimated spectrophotometrically (GENESYS 20 spectrophotometer, Thermo Fisher Scientific). The absorbance difference A (535–600 nm) was converted to MDA equivalents using the extinction coefficient for MDA 1.55×10^5 $M^{-1}cm^{-1}$. Lipid peroxidation was expressed in mM MDA.

2.2.2.3. Estimation of protein carbonyl content

The assessment of the protein carbonyl content (as an indicator of protein damage following oxidative stress) was evaluated in H9c2 cells by 2,4 dinitrophenylhydrazine (DNPH) assay, following the method of Reznick and Packer (1994) [28] and as previously described [26, 27]. Cells were seeded in a 24-well plate at a density of 1×10^5 cell/ml and treated as described above for 6 h. Subsequently, they were washed with cold PBS, centrifuged at 300 × g for 10 min and the supernatant was removed. The precipitate obtained was resuspended in 1 mL of a cold phosphate buffer 50 mM, pH 6.7, containing 1 mM ethylenediaminetetraacetic acid and crushed by ultrasonic wave. The protein carbonyl content (expressed in µM) was evaluated spectrophotometrically (GENESYS 20 spectrophotometer, Thermo Fisher Scientific) by absorbance detected at 375 nm, using the extinction coefficient for DNPH (22 mM^{-1} cm^{-1}).

2.2.2.4. Superoxide dismutase (SOD) enzyme activity assay

SOD activity was determined by measuring the inhibition of pyrogallol autoxidation following the method of Marklund S. and Marklund G. (1974) [29] and as previously described [30]. The cells were seeded in a 24-well plate at a density of 1×10^5 cell/ml and treated as described above for 6 h. Subsequently, the cells were washed with cold PBS, centrifuged at 300 × g for 10 min and the supernatant was removed. The precipitate obtained was resuspended in Tris buffer 50 mM, pH 8.2, containing 100 mM ethylenediaminetetraacetic acid and the reaction was initiated by adding 8 mM pyrogallol (prepared in 1 mM HCl). The SOD activity in the cell extract was measured by monitoring the autoxidation of pyrogallol for 5 min at room temperature using

a GENESYS 20 spectrophotometer (Thermo Fisher Scientific) at 420 nm. SOD activity was assessed as the degree of inhibition of the pyrogallol autoxidation rate.

2.2.3. Western blot

At the end of treatments with vehicle (control), LPS (10 µg/mL), LPS + *L*-Ctl (1 nM) and *L*-Ctl (1 nM) alone, the H9c2 cardiomyocytes were washed with DPBS (Gibco) and the proteins were extracted using RIPA lysis buffer (Sigma Aldrich) suitably supplemented with a mixture of protease inhibitors [(aprotinin 20 µg/mL, phenylmethylsulfonyl fluoride 1%, sodium orthovanadate 2 µM (Sigma-Aldrich)]. Cells were scraped and transferred in microcentrifuge tubes, incubated on ice for 30 min with intermittent mixing, and then centrifugated at 12,000 *g* for 15 min at 4°C. The supernatant was collected for protein concentration determination by Bradford reagent using bovine serum albumin (BSA) as a standard. Equal amounts of protein (30 µg) were loaded on 10% SDS-PAGE gel [for toll like receptor 4 (TLR4), phospho-extracellular-signal-regulated kinase 1/2 (p-ERK1/2), ERK1/2, phospho-c-Jun N-terminal kinase 1/2 (p-JNK1/2), JNK1/2, p-p38 mitogen-activated protein kinase (p-p38 MAPK), nuclear factor kappa-light-chain-enhancer of activated B cells (NFkB) p52, p-NFkB p65, NFkB p65 and cyclooxygenase-2 (COX2)], exposed to electrophoresis, and transferred to polyvinyl difluoride membranes (GE Healthcare, Chicago, USA). Membranes were blocked in 5% non-fat dried milk at room temperature for 1 h, and then incubated overnight at 4°C with primary antibodies specific for the above antigens diluted 1:1000 (for TLR4, p-ERK1/2 and ERK1/2) or 1:500 (for p-JNK1/2, JNK1/2, p-NFkB p65, NFkB p65, NFkB p52 and COX2) in tris-buffered saline containing 0.2% Tween 20 (TBST) and 5% BSA.
Antibodies against β-actin, ERK1/2, JNK1/2, p38-MAPK and NFkB p65 were used as internal controls. Following incubation with primary antibodies, all membranes were washed three times with TBST for 5 min and then incubated with secondary antibodies at room temperature for 2 h (anti-mouse and anti-rabbit peroxidase-linked, Santa Cruz Biotechnology, California, USA), diluted 1:2000 in TBST containing 5% non-fat dried milk. Immunodetection was carried out using the enhanced chemiluminescence kit (GE Healthcare). Membranes were exposed to X-ray films (Hyperfilm ECL, Amersham), the densitometric analyses of the bands areas and the pixel intensity were performed and the background was subtracted. The analyses were carried out using ImageJ 1.6 (National Institutes of Health, Bethesda, Maryland) as previously described [31,32].

2.2.4. Molecular docking

The molecular docking engine Autodock Vina [33] was used to simulate the binding of *L*-Ctl to the myeloid differentiation protein 2 (MD-2), the partner protein of TLR4. The structure of MD-2 was extracted from the entry 4G8A of the Protein Data Bank [34], which reports the crystallographic conformation of the complex with human TLR4 (polymorphic variant D299G and T399I) and with several ligand species in the binding site. All these molecules, including crystallographic waters, were not considered in the docking. Human Ctl

(sequence SSMRLSFRARGYGFR, L-enantiomeric form) was built in extended conformation by using UCSF Chimera [35].

Since the conformational space of Ctl is too large to be explored in a single simulation run, the search was performed in a simplified way, in analogy with a protocol already described for simulating the docking of peptides [36,37]. Full flexibility was guaranteed to seven consecutive residues [38], and the internal degrees of freedom of the other eight were inhibited. The flexible region was then systematically varied along the peptide sequence, from the N to the C terminus (SSMRLSF, SMRLSFR, ..., ARGYGFR), for a total of nine distinct simulations. The search was performed in a volume (40 Å × 40 Å × 40 Å) larger than the binding site of MD-2, and with exhaustiveness much greater (8-32 times larger) than the default value [39,40].

2.2.5. Quantitative Reverse-Transcription Real-Time PCR (qRT-PCR)

H9c2 cells were grown in 6-well plate to 70-80% confluence and then treated with vehicle (control), LPS (10 µg/mL), LPS + *L*-Ctl (1 nM) and *L*-Ctl (1 nM) alone. Total RNA from cells was isolated using TRIzol reagent (Invitrogen, Life Technologies, Carlsbad, CA, USA) according to the manufacturer's protocol. The purity and integrity of RNA were confirmed by spectrophotometric analysis.

1 µg of total RNA was reverse transcribed to provide complementary DNA (cDNA) using High-Capacity cDNA Reverse Transcription Kit (Applied Biosystems™, Thermo Fisher Scientific). The cDNA was amplified by qRT-PCR using SYBR™ Select Master Mix (Thermo Fisher Scientific) according to the manufacturer's instructions on Applied Biosystems™ QuantStudio™ 5 Real-Time PCR System apparatus (Thermo Fisher Scientific). Samples were analyzed in triplicate (n=3 independent experiments) and the relative mRNA expression levels of the different genes were normalized to rRNA18S and calculated on the basis of the $2^{-\Delta\Delta Ct}$ method [41,42].

Primers used for the amplification were: forward 5′-CCCAGGACATGCTAGGGAGCC-3′ and reverse 5′-AGGCAGGGAGGGAAACACACG-3′ (IL-1β); forward 5′-TGGAGTTCCGTTTCTACCTGG-3′ and reverse 5′-GGTCCTTAGCCACTCCTTCTGT-3′ (IL-6); forward 5′-CACCACGCTCTTCTGTCTACTG-3′ and reverse 5′-GCTACGGGCTTGTCACTCG-3′ (TNF-α); forward 5′-AGCCCTCACCTACTTCCTGG-3′ and reverse 5′-CTCTGCCTGTGCGTCTCTTC-3′ (NOS2); forward 5′-GCAATTATTCCCCATGAACG-3′ and reverse 5′-GGCCTCACTAAACCATCCAA-3′ (18S).

2.2.6. Statistical Analysis

Data, expressed as mean ± SEM, were analysed by one-way ANOVA and the non-parametric Newman-Keuls Multiple Comparison Test (for post-ANOVA comparisons) and one-way ANOVA followed by Dunnett's Multiple Comparison Test when appropriate. Values of *p =<0.05, **p =<0.01, ***p =<0.001 were considered statistically significant. The statistical analysis was carried out using Graphpad Prism 5 (GraphPad Software, La Jolla, California, USA).

3. Results

3.1. Effect of *L*-Ctl and *D*-Ctl on cell proliferation in H9c2 cardiomyocytes

In order to evaluate the effects of catestatin-derived peptides, *L*-Ctl and *D*-Ctl, on cell viability, H9c2 cells were exposed to increasing concentrations of either peptide species and the MTT was performed. As shown in **Figure 1A**, *L*-Ctl induced a significant increase in cell proliferation to each concentration tested (1-100 nM), while *D*-Ctl produced a significant increase in cardiac cell viability only at 5 nM, 10 nM and 100 nM (**Figure 1B**).

3.2. Action of *L*-Ctl and *D*-Ctl on LPS-induced damage in H9c2 cells

The action of *L*-Ctl or *D*-Ctl on LPS-induced injury in H9c2 cardiac cells was then investigated. To this aim, the cells were treated with LPS alone and in combination with increasing concentrations of *L*-Ctl or *D*-Ctl and cell viability was evaluated (**Figure 2**). MTT revealed that the treatment with LPS was able to significantly reduce cardiomyocytes viability; however, the cytotoxic effect exerted by LPS was reversed by both *L*-Ctl (**Figure 2A**) and *D*-Ctl (**Figure 2B**) treatments. In particular, *L*-Ctl induced beneficial effects on LPS-dependent cytotoxicity starting from 1 nM, and its effect was significant at each concentration tested (up to 100 nM) (**Figure 2A**). In contrast, *D*-Ctl reduced the H9c2 mortality when co-administered with LPS, only in the concentration range 10-100 nM (**Figure 2B**). Scrambled *L*-Ctl and *D*-Ctl were used as negative controls. **Figure 3** indicates that scrambled *L*-Ctl was inactive, since no significant effects have been observed on viability of H9c2 cells at the concentrations range of 1-100 nM, in the absence (**Figure 3A**) or in the presence of LPS (**Figure 3B**). Comparable data were obtained with the scrambled *D*-Ctl (data not shown).

3.3. Influence of *L*-Ctl on TLR4 expression in LPS-stimulated H9c2

Among the two Ctl enantiomers, *L*-Ctl has been showed to be more active (1 nM, that is referred to the first effective concentration) compared to *D*-Ctl (10 nM, that is referred to the first effective concentration) in the presence of LPS. Therefore, the cardiac molecular mechanism of *L*-Ctl was investigated. Western blot and densitometric analyses of cell extracts showed that TLR4 expression was significantly increased in LPS-treated cells with respect to the control group, whereas in the LPS + *L*-Ctl group the protein expression was reduced (**Figure 4**).

3.4. Molecular docking

Molecular docking was used to investigate whether the presence of *L*-Ctl can affect TLR4. Bacterial lipopolysaccharide and its precursor lipid A, as well as peptidomimetics with no structural similarity to the physiological ligands of TLR4, do not bind this protein directly but anchor in the relatively large binding site of its co-receptor MD-2 [34,43]. The conformation of MD-2 is similar in all these complex, and they only differ by the molecular contacts formed with the various ligands. Thus, we performed the molecular docking

of *L*-Ctl to a monomer of MD-2 extracted from a complex with human TLR4 [34], and isolated from any other molecular species.

Ctl possesses 15 amino acid residues and 64 rotatable dihedral angles, which is a number far too large to be exhaustively explored in a single molecular docking run. Therefore, the conformational space of the peptide was explored in a simplified way, by allowing rotations in the main and side chains of seven consecutive residues while the other eight residues were considered rigid, and systematically varying such flexible region along the whole peptide sequence.

The results indicated that the central region of *L*-Ctl (sequence fragment LSFRARG) has the most favorable affinity for MD-2, with a predicted binding energy of -10 kcal/mol. In contrast, the two peptide endings showed a comparatively lower binding score, with -8 kcal/mol for the N-terminal region and -8.5 kcal/mol for the C-terminal one. Due to the fact that the rigid portion of peptide structure was not optimized in the simulations, these values should be considered as an upper limit for the (negative) binding energy, and may reflect an even more favorable binding. The overall findings suggest a high affinity of *L*-Ctl for MD-2, with a binding equilibrium constant in the nanomolar range. **Figure 5** shows the structure or the most favorable docking pose of *L*-Ctl to MD-2 obtained in the simulations. The peptide is deeply inserted in the core of the protein binding site, and its position mostly overlaps with the location of the physiological ligands [34] in the original crystallographic complex.

3.5. Involvement of inflammatory pathways in *L*-Ctl mechanism of action

Western blot and densitometric analyses of H9c2 cell extracts were carried out to determine the expression levels of p-ERK1/2 (**Figure 6A**), p-JNK1/2 (**Figure 6B**), p-p38 MAPK (**Figure 6C**), NFkB p65 (**Figure 6D**), NFkB p52 (**Figure 6E**) and COX2 (**Figure 6F**) in H9c2 cells treated with LPS in the presence or absence of *L*-Ctl. The expression of all the above proteins significantly increased following LPS treatment and significantly decreased in the cells treated with LPS + *L*-Ctl (**Figure 6**).

3.6. Effect of *L*-Ctl on mRNA expression levels of inflammatory mediators

The *L*-Ctl molecular effect on the LPS-injured H9c2 cells was further investigated by assessing the mRNA expression levels of selective inflammatory mediators. qRT-PCR analysis of cell extracts revealed that the proinflammatory factors IL-1β (**Figure 7A**), IL-6 (**Figure 7B**), TNF-α (**Figure 7C**) and NOS2 (iNOS) (**Figure 7D**) were significantly upregulated in LPS-stimulated H9c2 cells compared with the control group. On the contrary, the mRNA expression levels of the above markers were significantly reduced in LPS + *L*-Ctl experimental group.

3.7. Effect of *L*-Ctl on oxidative stress-related markers, SOD activity and LDH release in H9c2 exposed to LPS

To determine whether *L*-Ctl could affect the cellular oxidative balance under LPS treatment, oxidative stress-related markers and the activity of the antioxidant enzyme SOD were measured. The MDA production and

342 the content of protein carbonyl groups, used as lipid peroxidation and protein damage markers, respectively,
343 were assayed in H9c2 cell lysates. **Figure 7** shows that MDA concentration (**Figure 7A)** and protein
344 carbonyl groups content (**Figure 7B)** were significantly increased in LPS group compared to the control,
345 while they were significantly decreased in the LPS + *L*-Ctl co-treatment. On the contrary, the percentage of
346 pyrogallol autoxidation (i.e. index of SOD activity) was significantly decreased in LPS-exposed H9c2, and
347 significantly increased in the LPS + *L*-Ctl group (**Figure 7C**). *L*-Ctl alone did not exert significant effects on
348 the above parameters compared to the vehicle exposed cells (**Figure 7 A-C**). As depicted in **Figure 7D,** LPS
349 treatment also significantly increased LDH, whose release in the H9c2 culture medium is considered an
350 indicator for cell membrane damage, whereas the co-treatment with *L*-Ctl reversed, to a significant extent,
351 the enzyme concentration released in response to LPS. *L*-Ctl treatment alone did not induce significant effect
352 in the LDH release compared to the control group (**Figure 7D**).

353 **4. Discussion**

354 The present study aimed to investigate the possible protective effects of Ctl in LPS-stimulated H9c2
355 cardiomyocytes. For the first time, we demonstrated that both *L*-Ctl and *D*-Ctl significantly increase cell
356 viability under LPS stimulation. Since the *L*-enantiomeric form of the peptide resulted more effective, it was
357 used for the subsequent analyses of the underlying mechanism of action. Our simulation results suggested
358 that Ctl may influence the biological activity of TLR4 through a direct binding to the partner protein MD-2.
359 In addition, molecular analyses showed that *L*-Ctl mitigates the LPS-dependent oxidative stress, the
360 reduction of SOD activity and the release of LDH in the cell medium. The peptide is also able to decrease the
361 expression of inflammatory signaling molecules (IL-1β, IL-6, TNF-α, iNOS) and the activation of important
362 inflammatory mediators (p-ERK 1/2, p-JNK, p-p38 MAPK, p-NFkB p65, p-NFkB p52, COX2). These data
363 are of interest in the context of myocarditis and in the field of antimicrobial peptides (AMPs) in regard to
364 their capability to counteract antibiotic resistance.
365 Antibiotic resistance, primarily due to the overuse of these drugs, has emerged as a severe worldwide health
366 problem, as every year millions of people are affected by multi-drug resistant bacteria resulting in a high
367 case-fatality ratio. For this reason, growing energies and efforts are invested in this field trying to reduce
368 antibiotic prescription and to identify or design alternative drugs able to overcome resistance. Among the
369 molecules currently considered as novel anti-infective agents [44], a prominent position is occupied by
370 AMPs, major players in the innate defense, since they have a relatively low chance to establish resistance
371 [45]. AMPs exist across all major lineages, they represent highly conserved forms of innate immunity and
372 are active against numerous pathogens [46]. Their short amphipathic -cationic conformation seems to be a
373 key component of their antimicrobial activity, since it promotes the disruption of microbial membranes [47].
374 In particular, mammalian AMPs are able to directly kill the microbe and activate rapidly the immune
375 response [48].

376 Ctl, the shorter and active arginine rich N-terminus fragment of CgA-derived Cst peptide, can be fully
377 included among AMPs, being effective against many microbial strains [18-20]. In the present study we tested

on an *in vitro* model of myocarditis, i.e. LPS-stimulated H9c2 cells [49], both the naturally occurring enantiomeric species *L*-Ctl and its derived epipeptide *D*-Ctl, where all *L*-amino acids have been replaced by *D*-amino acids. In this regard, it is known that LPS, expressed on the external membrane of Gram-negative bacteria, represents a powerful inducer of immunity responses through the modulation of toll-like receptors 4 (TLR4) [7]; for this reason, it is widely used to reproduce inflammatory diseases, such as myocarditis [50]. Myocarditis, or inflammatory cardiomyopathy, is an inflammatory condition of the myocardium that, if prolonged, leads to cardiac injury, cardiac dysfunction, cardiomyocytes death [49] and resistance of the infectious agents to therapies [51].

In our experimental model, both *L*-Ctl and *D*-Ctl were able to improve cell viability, alone or when administered together with LPS, while their scrambled *L*-Ctl and *D*-Ctl counterparts were unable to significantly affect cell viability. Indeed, according to previous data [52], LPS alone reduces cell viability and induces a significant release of LDH (an indicator of cytotoxicity) in the culture medium, indicating that the model of myocarditis has been successfully established. Of note, *L*-Ctl showed greater effectiveness with respect to the *D*-enantiomeric form in increasing cell viability and in relieving LPS effects at all the tested concentrations. *D*-Ctl was produced, starting from its natural peptide, to promote the stability of the peptide against bacterial proteases and, at variance with our results, it was much more effective against microbial strains and more resistant to proteolytic degradation than *L*-Ctl [18,20]. Nevertheless, our study did not include a microbiology approach but aimed to analyze an *in vitro* model of myocarditis and this may account for the different potency observed for *D*-Ctl and *L*-Ctl in these diverse experimental sets. Moreover, it is conceivable that, from a physiological point of view, H9c2 cells establish a more favorable interactions with the natural occurring *L*-Ctl, since molecular chirality is a key feature in molecular host-guest recognition [53]. Results have been further corroborated by the use of a scrambled/inert peptide.

Thus, we focused on the anti-bacterial/anti-inflammatory role of *L*-Ctl possibly mediated via the TLR4 pathway. It is well established that LPS activates TLR4 and its downstream cascade by the interaction with its essential accessory protein, namely MD-2 [54]. LPS binds the hydrophobic pocket of MD-2 through 5 of its acyl chains, allowing the engagement and the dimerization of TLR4 and the generation of the activated LPS-MD2-TLR4 complex [54]. The crucial role of MD-2 in TLR4 inflammatory responses has been supported by studies performed on MD-2 knockout mice, that showed hypo-responsiveness to LPS and higher rate of survival to endotoxic shock [55]. Confirming previous experimental evidences, in our model LPS induces an increase in TLR4 protein expression, generally regulated by transcriptional and post-transcriptional mechanisms [56]. This supports the important contribution of TLR4 to the relationship existing between inflammation and cardiovascular disorders. Since *L*-Ctl was able to mitigate the LPS-dependent upregulation of TLR4, it is conceivable that a regulation of its expression at the MD-2 level may exist. Accordingly, the molecular docking analysis clearly supported the interaction between the peptide and MD-2, the TLR4 partner protein. Indeed, the results of our computational studies suggest a high affinity of *L*-Ctl for MD-2, with a predicted binding energy of at least -10 kcal/mol. The peptide deeply plunged into

414 the protein binding site with residues Phe7, Arg8 and Arg10. It is likely that the energetic penalty due to the
415 desolvation of the arginine side chains buried into the protein pocket was adequately compensated by
416 electrostatic and entropic effects at the peptide termini, which are exposed and relatively free to fluctuate in
417 the solvent, although such effects cannot be directly assessed by using molecular docking. A number of
418 interactions stabilized the anchoring of the peptide into MD-2, including electrostatic attraction with the
419 charged residue Glu92 of the protein, and hydrophobic interactions with several phenylalanine isoleucine
420 residues. Thus, our simulation results strongly suggest the possibility that Ctl may influence the biological
421 activity of TLR4 through a direct binding to the partner protein MD-2. Both the interaction energy and the
422 predicted location of binding of Ctl are fully consistent with an anchoring in the protein pocket, similar to the
423 one observed in the experiment for physiological ligands bound to MD-2. The interaction between Ctl and
424 MD-2 could thus represent the mechanism used by the peptide to suppress LPS inflammation, since a
425 competitive antagonism on this site can be postulated.

426 It is widely accepted that the activation of TLR4, such as under LPS stimulation, induces the downstream
427 MAPKs cascade converging on NFkB, lastly able to promote the expression of pro-inflammatory actors,
428 including IL-1β, IL-6, TNF-α, NOS2 [57,58]. Of note, Ctl downregulates the expression of these proteins
429 corroborating its supposed anti-inflammatory action via TLR4 inhibition.

430 Moreover, it is known that NFkB importantly participates in immune responses [59] and its overactivation
431 contributes to the long-term inflammation responsible for acute myocardial lesions [60]. Indeed, NFkB is a
432 well established downstream player of LPS/TLR4, MAPKs and JNK activation [56,61,62], and a positive
433 regulator of COX2 expression, a key enzyme of inflammatory pathways [63]. Accordingly, our results
434 showed an increase of p-ERK 1/2, p-JNK, p-NFkB p65, p-NFkB p52, and inducible COX under LPS
435 stimulation, reversed by the addition of *L*-Ctl to the medium. Therefore, it is plausible that *L*-Ctl, by reducing
436 the LPS-induced NFkB expression, may also prevent the production and the release of proinflammatory
437 cytokines in cardiac myocytes [64], as showed in our experimental set. This finding can be further supported
438 by evidences indicating the ability of another CgA-derived peptide (chromofungin, CgA $_{47–66}$) to exert
439 antiinflammatory effects by inhibiting the NFkB-mediated transcription [65]. Interestingly, in our LPS-
440 stimulated model p38 MAPK is more phosphorylated, according to the increased expression of NFkB,
441 conversely to what happens under Ctl treatment. Being NFkB a crucial target for MAP-kinases, such as p38
442 MAPK that is strongly involved in cardiac pathologies [66 and references therein], this result may be useful
443 in the view of future frontiers in therapeutics.

444 Another important aspect regards the well established ROS production, and its resulting oxidative stress,
445 detectable in septic myocardial inflammation [67,68]. According to these data, in our model LPS is a strong
446 stimulus for oxidative stress as visible by the increase of MDA and of protein carbonylation (used as markers
447 of lipid peroxidation and protein damage secondary to oxidative stress, respectively) and by the reduction of
448 SOD activity. The amelioration of oxidative balance following *L*-Ctl treatment, further describes the peptide
449 as a novel candidate in the treatment of septic cardiomyopathy. Moreover, in line with our results, LPS-

induced oxidative stress may additionally contribute to the activation of NFkB that, in turn, may further impact the cardiomyocytes inflammation that is finally mitigated/abolished by Ctl.

5. Conclusions

Taken together our results describe Ctl as a potential anti-inflammatory/anti-microbial therapeutic agent, and its inhibition of TLR4 by targeting MD-2 could represent an effective tool to counteract sepsis and septic shock induced by Gram negative bacteria in addition to its interesting and protective antioxidant properties. These data are of interest considering that Ctl efficacy and resistance have been extensively demonstrated in several microbial strains. Moreover, being a short and linear peptide, stable in a wide range of pH and temperature, Ctl would be easily synthesized at a minimal cost making it an excellent candidate for future drug development.

Author Contributions

The individual contributions of the authors are specified as follows: Conceptualization, Carmine Rocca and Tommaso Angelone; Data curation, Carmine Rocca, Anna De Bartolo, Fedora Grande, Bruno Rizzuti, Teresa Pasqua, Francesca Giordano, Maria Concetta Granieri, Maria Antonietta Occhiuzzi and Nicola Amodio; Methodology, Carmine Rocca, Anna De Bartolo, Fedora Grande, Bruno Rizzuti, Teresa Pasqua, Francesca Giordano, Maria Concetta Granieri, Maria Antonietta Occhiuzzi and Nicola Amodio; Supervision, Marie-Hélène Metz-Boutigue and Tommaso Angelone; Validation, Carmine Rocca, Anna De Bartolo, Fedora Grande, Bruno Rizzuti, Teresa Pasqua, Francesca Giordano, Maria Concetta Granieri, Maria Antonietta Occhiuzzi, Nicola Amodio and Tommaso Angelone; Writing – original draft, Carmine Rocca, Anna De Bartolo, Fedora Grande, Bruno Rizzuti, Teresa Pasqua and Tommaso Angelone; Writing – review & editing, Antonio Garofalo, Nicola Amodio, Maria Carmela Cerra, Francis Schneider, Maria Luisa Panno and Marie-Hélène Metz-Boutigue. All authors have read and approved the final version of the manuscript.

Funding

This work was supported by the Ministry of Education, University and Research (MIUR) of Italy (ex 60%), Inserm UMR 1121 (France) and Doctorate School in “Life Science and Technology” (Italy).

Acknowledgments

C.R. acknowledges POR Calabria (Italy) FESR-FSE 2014/2020-Azione 10.5.12-Linea B (DR n. 683 del 21/05/2019) for financial support for RTDa position. B.R. acknowledges the use of computational resources from the European Magnetic Resonance Center (CERM), Sesto Fiorentino (Florence), Italy. T.P. acknowledges PON “Ricerca e Innovazione” 2014–2020: AIM “Attraction and International Mobility” (MIUR, Italy) for financial support for RTDa position.

Conflicts of Interest

The authors declare no conflicts of interest.

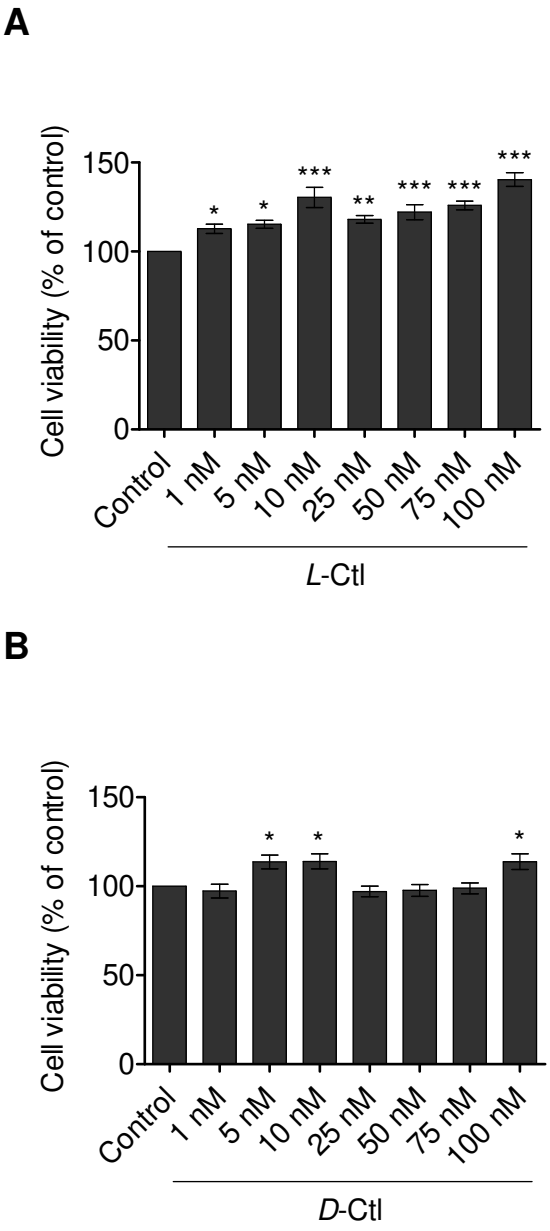


Figure 1. Effects of *L*-cateslytin (*L*-Ctl) and *D*-cateslytin (*D*-Ctl) on cell viability in H9c2 cardiomyocytes.

H9c2 cardiomyocytes were treated with vehicle (Control) or increasing concentration of **A)** *L*-Ctl (1-100 nM) or **B)** *D*-Ctl (1-100 nM) for 6 h. Cell viability was determined using MTT assay and was expressed as the percentage of control cells only exposed to vehicle (indicated as Control). Results are represented as mean ± SEM (n=6 per group). Significant differences were detected by one-way ANOVA followed by Dunnett's test, *$p<0.05$ (*); $p<0.01$ (**) and $p<0.001$ (***) vs* Control group.

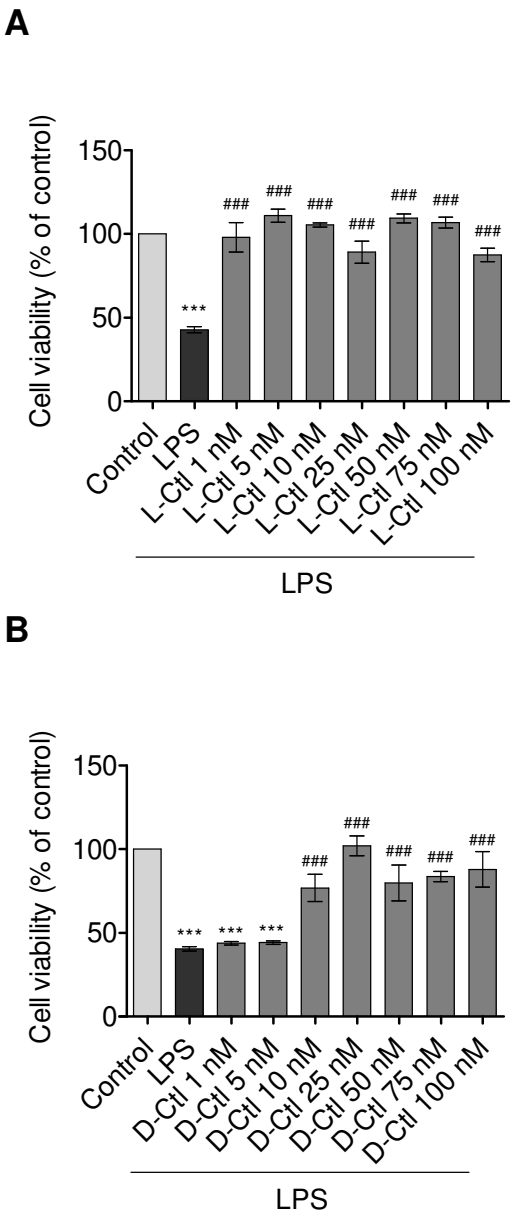


Figure 2. Effects of *L*-Ctl and *D*-Ctl in the presence of lipopolysaccharide (LPS) on H9c2 cardiomyocytes viability.

H9c2 cardiomyocytes were treated with vehicle (Control) or LPS (10 µg/mL) alone and in co-treatment with increasing concentration of **A)** *L*-Ctl (1-100 nM) or **B)** *D*-Ctl (1-100 nM) for 6 h. Cell viability was determined using MTT assay and was expressed as the percentage of control cells only exposed to vehicle (indicated as Control). Results are represented as mean ± SEM (n=6 per group). Significant differences were

detected by one-way ANOVA and Newman-Keuls multiple comparison test. *p<0.001 (***) vs* Control group; *p<0.001 (###) vs* LPS group.

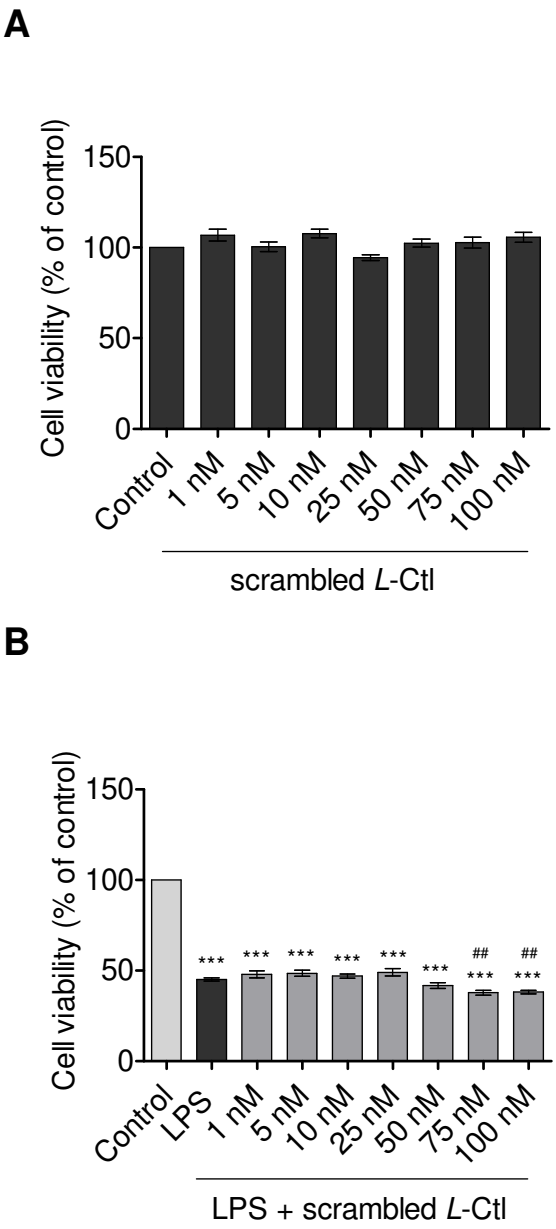


Figure 3. Effect of scrambled *L*-Ctl in the absence or in the presence of LPS on H9c2 cardiomyocytes viability

H9c2 cardiomyocytes were treated with vehicle (Control) or increasing concentration of scrambled *L*-Ctl (1-100 nM) for 6 h **A)** Cell viability was determined using MTT assay and was expressed as the percentage of control cells only exposed to vehicle (indicated as Control). Results are represented as mean ± SEM (n=6 per group). Statistical analysis was carried out by one-way ANOVA followed by Dunnett's test.

H9c2 cardiomyocytes were treated with vehicle (Control) or LPS (10 µg/mL) alone and in co-treatment with increasing concentration of scrambled *L*-Ctl (1-100 nM) for 6 h **B)** Significant differences were detected by one-way ANOVA and Newman-Keuls multiple comparison test. *p<0.001 (***) vs* Control group; *p<0.01 (##) vs* LPS group.

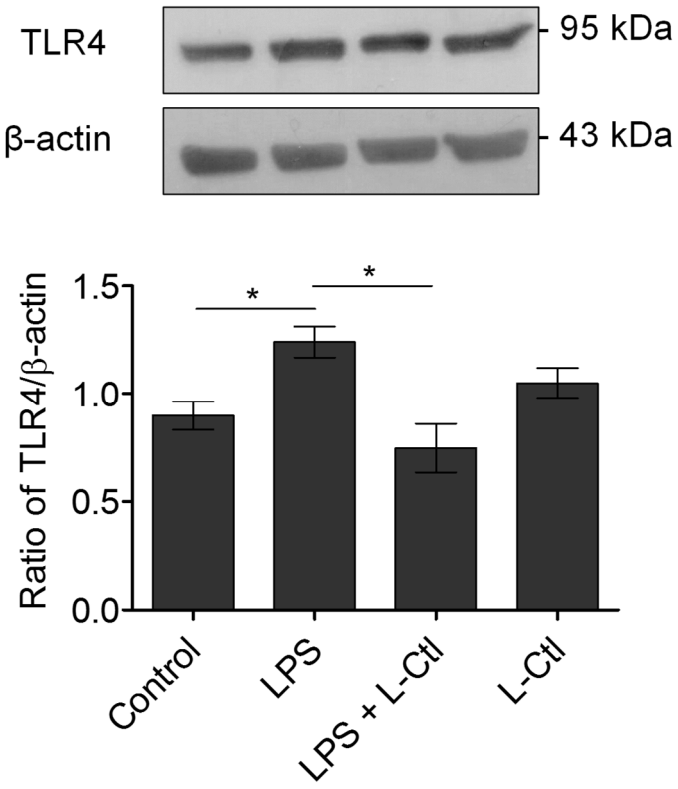


Figure 4. Influence of *L*-Ctl on toll like receptor 4 (TLR4) expression in H9c2 cardiomyocytes stimulated with LPS.

Western blot analysis of TLR4 in H9c2 cardiomyocytes exposed to vehicle (indicated as Control), LPS (10 µg/mL), LPS + *L*-Ctl (1 nM) (n=3 independent experiments) [mouse monoclonal antibody against TLR4 (Cat# sc-293072, RRID:AB_10611320) and β-actin (Cat# sc-69879, RRID:AB_1119529) Santa Cruz Biotechnology (Dallas, Texas, USA)]. Histograms represent the ratio of densitometric analysis of protein:loading control. Significant differences were detected by one-way ANOVA and Newman-Keuls multiple comparison test. *p <0.05 (*).*

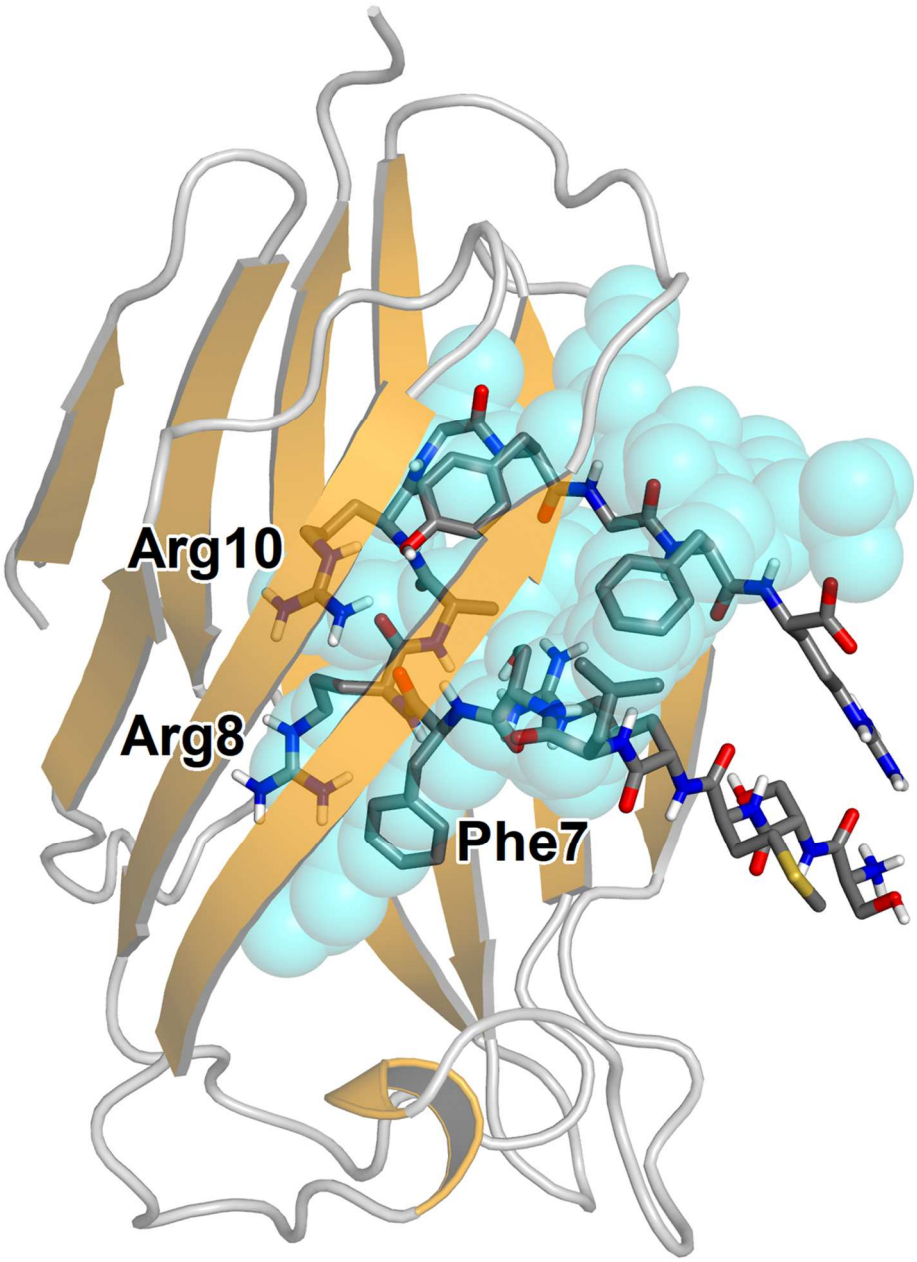


Figure 5. Binding of Ctl to myeloid differentiation factor 2 (MD-2).

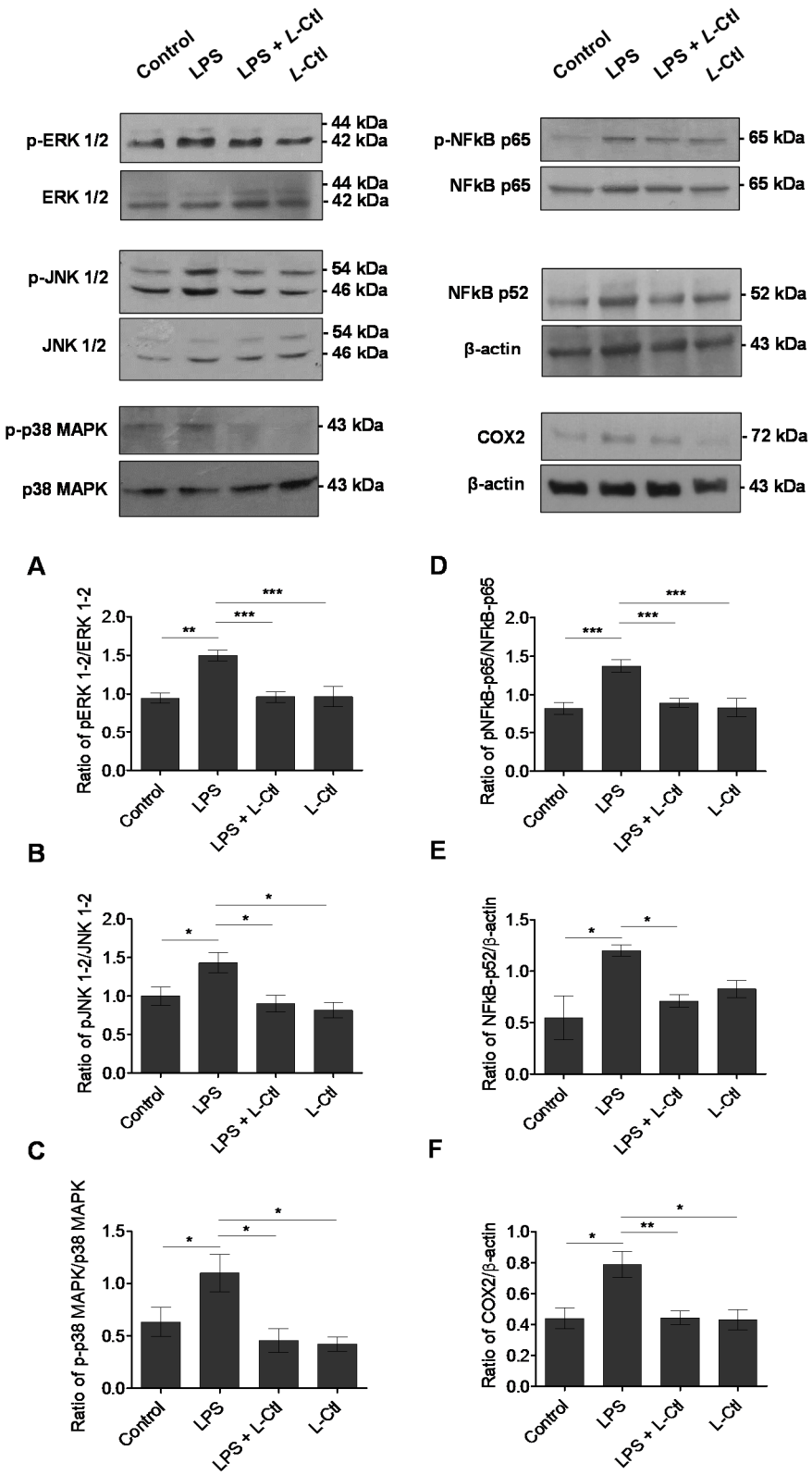
Most favorable structure of Ctl (stick representation, with colored atoms) bound in the binding site of MD-2 (yellow cartoon representation), superimposed to the volume occupied in the same pocket by physiological ligands (cyan spheres) in the crystallographic structure of the protein [34]. Image created with PyMol [69].

548

549

550

551



552

Figure 6. Molecular mechanism activated by *L*-Ctl in H9c2 cardiomyocytes.

Western blot analysis of **A)** phospho- extracellular-signal-regulated kinase 1/2 (p-ERK1/2), **B)** phospho-c-JunN-terminal kinase 1/2 (p-JNK1/2), **C)** phospho-p38 mitogen-activated protein kinase (p38 MAPK), **D)** nuclear factor kappa-light-chain-enhancer of activated B cells (NFkB) p65 (p-NFkB p65), **E)** NFkB p52 and **F)** cyclooxygenase-2 (COX2) in H9c2 cardiomyocytes exposed to vehicle (indicated as Control), LPS (10 µg/mL), LPS + *L*-Ctl (1 nM) and *L*-Ctl (1 nM) (n=3 independent experiments) for 6 h [mouse monoclonal antibodies against p-ERK1/2 (Cat# sc-7383), ERK1/2 (Cat# sc-514302), NFkB p65 (Cat# sc-8008), NFkB p52 (Cat# sc-7386, RRID:AB_2267131) Santa Cruz Biotechnology (Dallas, Texas, USA), p-NFkB p65 (#13346), Cell Signaling Technology, Inc, (Danvers, Massachusetts, USA), or rabbit polyclonal antibodies against p-SAPK/JNK (#9251), SAPK/JNK (#9252), p-p38 MAPK (#9211) or p38 MAPK (#9218), Cell Signaling Technology, or COX2 (Cat# TA313292), OriGene Technologies (Rockville, Maryland, USA)]. Histograms represent the ratio of densitometric analysis of protein:loading control. Significant differences were detected by one-way ANOVA and Newman-Keuls multiple comparison test. *p <0.05 (*); p <0.01 (**); p<0.001 (***).*

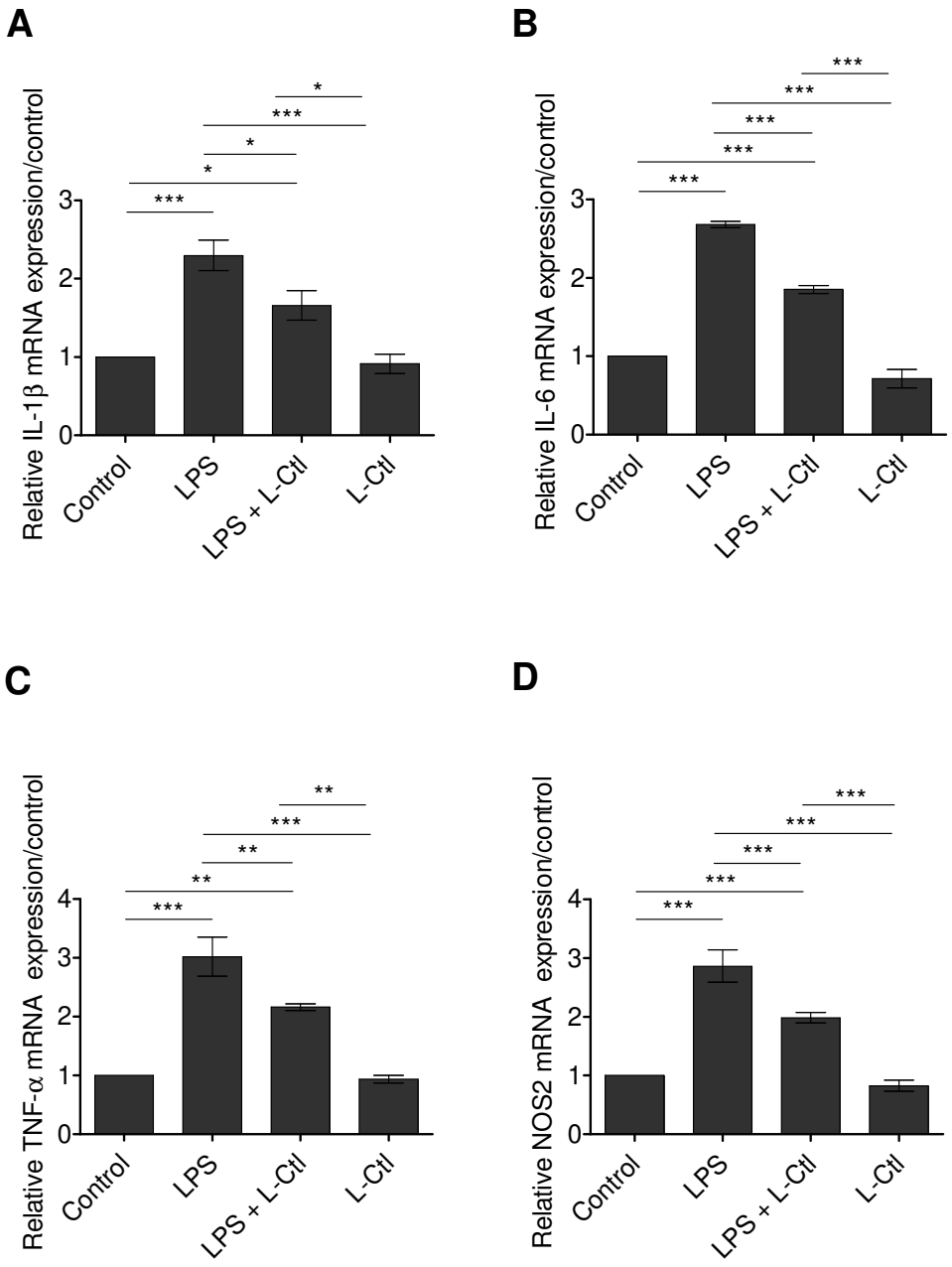


Figure 7. Effects of *L*-Ctl on the LPS-induced mRNA expression of inflammatory mediators in H9c2 cells.

Evaluation of mRNA expression levels of **A)** interleukin (IL)-1β, **B)** IL-6, **C)** tumor necrosis factor (TNF)-α, and **D)** nitric oxide synthase (NOS) 2 (inducible) by quantitative reverse-transcription real-time PCR (qRT-PCR) in H9c2 cardiomyocytes exposed to vehicle (indicated as Control), LPS (10 µg/mL), LPS + *L*-Ctl (1 nM) and *L*-Ctl (1 nM) for 6 h. Samples were analyzed in triplicate, the relative mRNA expression levels of the different genes were normalized to rRNA18S and calculated on the basis of the $2^{-\Delta\Delta Ct}$ method. Data are expressed as the mean ± SEM of 3 separate experiments. Significant differences were detected by one-way ANOVA and Newman-Keuls multiple comparison test. *$p < 0.05$ (*); $p < 0.01$ (**); $p < 0.001$ (***).*

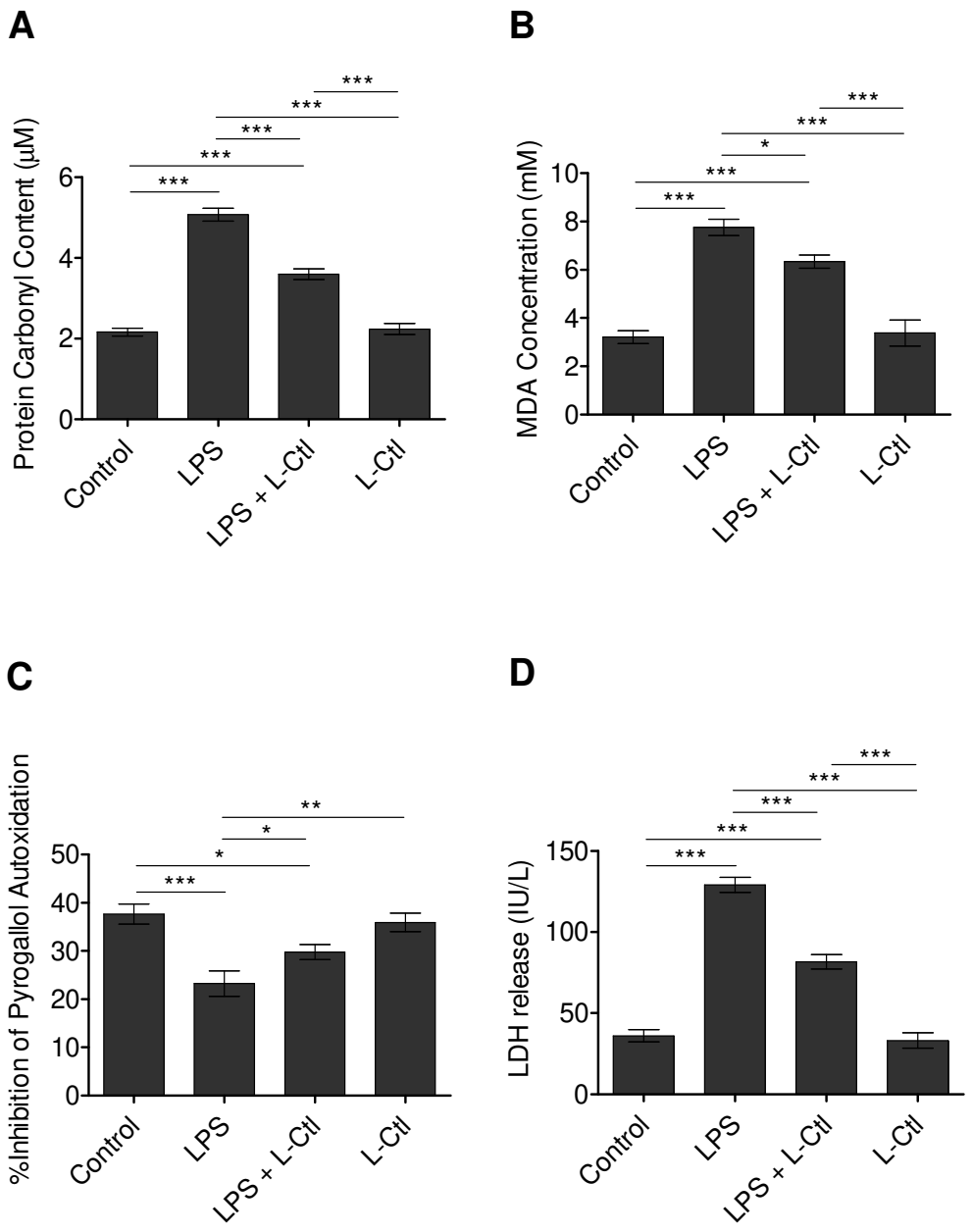


Figure 8. Effect of *L*-Ctl on malondialdehyde (MDA) levels, protein carbonyl groups content, superoxide dismutase (SOD) activity and lactate dehydrogenase (LDH) release in LPS-treated H9c2 cells.

MDA concentration **A)**, protein carbonyl groups content **B)** and SOD activity **C)** in lysates of H9c2 cardiomyocytes treated with vehicle (Control), LPS (10 µg/mL), LPS + *L*-Ctl (1 nM) and *L*-Ctl (1 nM) for 6 h. MDA concentration was expressed as mmol/L, protein carbonyl groups content was expressed as µmol/L and SOD activity was expressed as percentage of inhibition of the pyrogallol autoxidation rate. Data are expressed as the mean ± SEM of six separate experiments. Significant differences were detected by one-way ANOVA and Newman-Keuls multiple comparison test. *$p < 0.05$ (*); $p < 0.01$ (**); $p < 0.001$ (***).* LDH

release in the supernatant of H9c2 cardiomyocytes treated with vehicle (Control), LPS (10 µg/mL), LPS + L-Ctl (1 nM) and *L*-Ctl (1 nM) for 24 h **D)**. The result of LDH activity was expressed as IU/L. Data are expressed as the mean ± SEM of six separate experiments. Significant differences were detected by one-way ANOVA and Newman-Keuls multiple comparison test. *p <0.001 (***).*

References

[1] S.P. Caforio, E. Arbustini, C. Basso, J. Gimeno-Blanes, S.B. Felix, M. Fu, T. Heliö, S. Heymans, R. Jahns, K. Klingel, A. Linhart, B. Maisch, W. McKenna, J. Mogensen, Y.M. Pinto, A. Ristic, H.P. Schultheiss, H. Seggewiss, L. Tavazzi, G. Thiene, A. Yilmaz, P. Charron, P.M. Elliott, Current state of knowledge on aetiology, diagnosis, management, and therapy of myocarditis: a position statement of the European Society of Cardiology Working Group on Myocardial and Pericardial Diseases. Eur. Heart J. (2013), 2636-48. https://doi.org/10.1093/eurheartj/eht210.

[2] V.O. Puntmann, M.L. Carerj, I. Wieters, M. Fahim, C. Arendt, J. Hoffmann, A. Shchendrygina, F. Escher, M. Vasa-Nicotera, A.M. Zeiher, M. Vehreschild, E, Nagel, 2020. Outcomes of Cardiovascular Magnetic Resonance Imaging in Patients Recently Recovered From Coronavirus Disease 2019 (COVID-19). JAMA Cardiol., e203557. https://doi.org/10.1001/jamacardio.2020.3557.

[3] F. Moccia, A. Gerbino, V. Lionetti, M. Miragoli, L.M. Munaron, P. Pagliaro, T. Pasqua, C. Penna, C. Rocca, M. Samaja, T. Angelone, COVID-19-associated cardiovascular morbidity in older adults: a position paper from the Italian Society of Cardiovascular Researches. Geroscience (2020), 1-29. https://doi.org/10.1007/s11357-020-00198-w.

[4] A. Vieillard-Baron, V. Caille, C. Charron, G. Belliard, B. Page, F. Jardin, Actual incidence of global left ventricular hypokinesia in adult septic shock. Crit. Care Med. (2008), 1701-1706. https://doi.org/10.1097/ccm.0b013e318174db05.

[5] M.W. Merx, C. Weber, Sepsis and the heart. Circulation (2007), 793-802. https://doi.org/10.1161/CIRCULATIONAHA.106.678359.

[6] S. Frantz, L. Kobzik, Y.D. Kim, R. Fukazawa, R. Medzhitov, R.T. Lee, R.A. Kelly, Toll4 (TLR4) expression in cardiac myocytes in normal and failing myocardium. J. Clin. Invest. (1999), 271–280. https://doi.org/10.1172/JCI6709.

[7] Y. Yang, J. Lv, S. Jiang, Z. Ma, D. Wang, W. Hu, C. Deng, C. Fan, S. Di, Y. Sun, W. Yi, 2016. The emerging role of Toll-like receptor 4 in myocardial inflammation. Cell Death Dis., 7(5): e2234. https://doi.org/10.1038/cddis.2016.140e.

[8] R.N. Naylor, R. Atun, N. Zhu, K. Kulasabanathan, S. Silva, A. Chatterjee, G.M. Knight, J.V. Robotham, Estimating the burden of antimicrobial resistance: a systematic literature review. Antimicrob. Resist. Infect. Control. (2018), 7: 58. https://doi.org/10.1186/s13756-018-0336-y.

[9] M. Mateescu, S. Baixe, T. Garnier, L. Jierry, V. Ball, Y. Haikel, M.H. Metz-Boutigue, M. Nardin, P. Schaaf, O. Etienne, P. Lavalle, 2015. Antibacterial Peptide- Based Gel for Prevention of Medical Implanted-Device Infection. PLoS One, 10(12), e0145143. https://doi.org/10.1371/journal.pone.0145143.

[10] D. Zhang, P. Shooshtarizadeh, B.J. Laventie, D.A. Colin, J.F. Chich, J. Vidic, J. de Barry, S. Chasserot-Golaz, F. Delalande, A. Van Dorsselaer, F. Schneider, K. Helle, D. Aunis, G. Prévost, M.H. Metz-Boutigue, 2009. Two Chromogranin A-Derived Peptides Induce Calcium Entry in Human Neutrophils by Calmodulin-Regulated Calcium Independent Phospholipase A2. PLoS One, 4(2), e4501. https://doi.org/ 10.1371/journal.pone.0004501.

[11] E. Glattard, T. Angelone, J.M. Strub, A. Corti, D. Aunis, B. Tota, M.H. Metz-Boutigue, Y. Goumon, Characterization of natural vasostatin-containing peptides in rat heart. FEBS J. (2006), 3311-3321. https://doi.org/10.1111/j.1742-4658.2006.05334.x.

[12] K.B. Helle, M.H. Metz-Boutigue, M.C. Cerra, T. Angelone, Chromogranins: from discovery to current times. Pflugers Arch (2018), 143-154. https://doi.org/10.1007/s00424-017-2027-6.

[13] T. Pasqua, C. Rocca, A. Spena, T. Angelone, M.C. Cerra, Modulation of the coronary tone in the expanding scenario of Chromogranin-A and its derived peptides. Future Med. Chem., Volume 11, Issue 12, 2019, Pages 1501-1511.

[14] T. Pasqua, A. Corti, S. Gentile, L. Pochini, M. Bianco, M.H. Metz-Boutigue, M.C. Cerra, B. Tota, T. Angelone, Full-length human chromogranin-A cardioactivity: myocardial, coronary, and stimulus-induced processing evidence in normotensive and hypertensive male rat hearts. Endocrinology (2013), 154(9):3353-65. https://doi.org/10.1210/en.2012-2210.

[15] J. Troger, M. Theurl, R. Kirchmair, T. Pasqua, B. Tota, T. Angelone, M.C. Cerra, Y. Nowosielski, R. Mätzler, J. Troger, J.R. Gayen, V. Trudeau, A. Corti, K.B. Helle, Granin-derived peptides. Prog Neurobiol. (2017), 154:37-61. https://doi.org/10.1016/j.pneurobio.2017.04.003.

[16] L. Taupenot, S.K. Mahata, M. Mahata, R.J. Parmer, D.T. O'Connor, Interaction of the catecholamine release-inhibitory peptide catestatin (human chromogranin A (352-372)) with the chromaffin cell surface and Torpedo electroplax: implications for nicotinic cholinergic antagonism. Regul. Pept. (2000), 9-17. https://doi.org/10.1016/s0167-0115(00)00135-x.

[17] E.M. Muntjewerff, G. Dunkel, M.J.T. Nicolasen, S.K. Mahata, G. van den Bogaart, Catestatin as a Target for Treatment of Inflammatory Diseases. Front. Immunol. (2018), 9: 2199. https://doi.org/10.3389/fimmu.2018.02199.

[18] P. Dartevelle, C. Ehlinger, A. Zaet, C. Boehler, M. Rabineau, B. Westermann, J.M. Strub, S. Cianferani, Y. Haïkel, M.H. Metz-Boutigue, C. Marban, D-Cateslytin: a new antifungal agent for the treatment of oral Candida albicans associated infections. Sci. Rep. (2018), 18; 9235. https://doi.org/10.1038/s41598-018-27417-x.

690 [19] R. Aslam, M. Atindehou, T. Lavaux, Y. Haïkel, F. Schneider, M.H. Metz-Boutigue, Chromogranin
691 A-derived peptides are involved in innate immunity. Curr. Med. Chem. (2012), 4115-4123.
692 https://doi.org/10.2174/092986712802430063.
693 [20] A. Zaet, P. Dartevelle, F. Daouad, C. Ehlinger, F. Quilès, G. Francius, C. Boehler, C. Bergthold, B.
694 Frisch, G. Prévost, P. Lavalle, F. Schneider, Y. Haïkel, M.H. Metz-Boutigue, C. Marban, D-
695 Cateslytin, a new antimicrobial peptide with therapeutic potential. Sci. Rep. (2017), 15199.
696 https://doi.org/10.1038/s41598-017-15436-z.
697 [21] C. Rocca, S. Femminò, G. Aquila, M.C. Granieri, E.M. De Francesco, T. Pasqua, D.C. Rigiracciolo,
698 F. Fortini, M.C. Cerra, M. Maggiolini, P. Pagliaro, P. Rizzo, T. Angelone, C. Penna, Notch1
699 Mediates Preconditioning Protection Induced by GPER in Normotensive and Hypertensive Female
700 Rat Hearts. Front. Physiol. (2018), 9-521. https://doi.org/10.3389/fphys.2018.00521.
701 [22] Y. Zheng, S. Li, R. Hu, F. Cheng, L. Zhang, GFI-1 Protects Against Lipopolysaccharide-Induced
702 Inflammatory Responses and Apoptosis by Inhibition of the NF-κB/TNF-α Pathway in H9c2 Cells.
703 Inflammation (2020), 74-84. https://doi.org/10.1007/s10753-019-01095-x.
704 [23] M.J. McQueen, Optimal Assay of LDH and α-HBD at 37 °C. Ann. Clin. Biochem. (1972), 9, 2.
705 https://doi.org/10.1177/000456327200900102.
706 [24] C. Rocca, F. Scavello, B. Colombo, A.M. Gasparri, A. Dallatomasina, M.C. Granieri, D. Amelio, T.
707 Pasqua, M.C. Cerra, B. Tota, A. Corti, T. Angelone, Physiological levels of chromogranin A prevent
708 doxorubicin-induced cardiotoxicity without impairing its anticancer activity. FASEB J. (2019),
709 7734-7747. https://doi.org/10.1096/fj.201802707R.
710 [25] S.F. Assimakopoulos, C.E. Vagianos, G. Zervoudakis, K.S. Filos, C. Georgiou, V. Nikolopoulou,
711 C.D. Scopa, Gut regulatory peptides bombesin and neurotensin reduce hepatic oxidative stress and
712 histological alterations in bile duct ligated rats. Regul. Pept. (2004), 185– 193.
713 https://doi.org/10.1016/j.regpep.2004.03.010.
714 [26] M.R. Preetha Rani, N. Anupama, M. Sreelekshmi, K.G. Raghu, Chlorogenic acid attenuates
715 glucotoxicity in H9c2 cells via inhibition of glycation and PKC α upregulation and safeguarding
716 innate antioxidant status. Biomed. Pharmacother. (2018), 467-4777.
717 https://doi.org/10.1016/j.biopha.2018.02.027.
718 [27] T. Pasqua, C. Rocca, F. R. Lupi, N. Baldino, D. Amelio, O. I. Parisi, M. C. Granieri, A. De Bartolo,
719 A. Lauria, M. Dattilo, I. D. Perrotta, F. Puoci, M. C. Cerra, D. Gabriele, T. Angelone, Cardiac and
720 Metabolic Impact of Functional Foods with Antioxidant Properties Based on Whey Derived Proteins
721 Enriched with Hemp Seed Oil. Antioxidants (2020), 9 (11) 1066.
722 https://doi.org/10.3390/antiox9111066.
723 [28] A.Z. Reznick, L. Packer, Oxidative damage to proteins: spectrophotometric method for carbonyl
724 assay. Methods Enzymol. (1994), 357-63. https://doi.org/10.1016/s0076-6879(94)33041-7.

[29] S. Marklund, G. Marklund, Involvement of the superoxide anion radical in the autoxidation of pyrogallol and a convenient assay for superoxide dismutase. Eur. J. Biochem. (1974), 469-74. https://doi.org/10.1111/j.1432-1033.1974.tb03714.x.

[30] A. Thakur, J. Alam M.R. Ajayakumar, S. Ghaskadbi, M. Sharma, S.K. Goswami, Norepinephrine-induced apoptotic and hypertrophic responses in H9c2 cardiac myoblasts are characterized by different repertoire of reactive oxygen species generation. Redox Biology (2015), 243-252. https://doi.org/10.1016/j.redox.2015.05.005.

[31] C. Rocca, L. Boukhzar, M.C. Granieri, I. Alsharif, R. Mazza, B. Lefranc, B. Tota, J. Leprince, M.C. Cerra, Y. Anouar, T Angelone, 2018. A selenoprotein T-derived peptide protects the heart against ischaemia/reperfusion injury through inhibition of apoptosis and oxidative stress. Acta Physiol., 223(4):e13067. https://doi.org/10.1111/apha.13067.

[32] C. Rocca, F. Scavello, M.C. Granieri, T. Pasqua, N. Amodio, S. Imbrogno, A. Gattuso, R. Mazza, M.C. Cerra, T. Angelone, Phoenixin-14: detection and novel physiological implications in cardiac modulation and cardioprotection. Cell. Mol. Life Sci. (2018), 743-756. https://doi.org/10.1007/s00018-017-2661-3.

[33] O. Trott, A.J. Olson, AutoDock Vina: Improving the speed and accuracy of docking with a new scoring function, efficient optimization, and multithreading. J. Comput. Chem. (2010), 455-461. https://doi.org/10.1002/jcc.21334.

[34] U. Ohto, N. Yamakawa, S. Akashi-Takamura, K. Miyake, T. Shimizu, Structural analyses of human Toll-like receptor 4 polymorphisms D299G and T399I. J. Biol. Chem. (2012), 40611-40617. https://doi.org/ 10.1074/jbc.M112.404608.

[35] E.F. Pettersen, T.D. Goddard, C.C. Huang, G.S. Couch, D.M. Greenblatt, E.C. Meng, T.E. Ferrin, UCSF Chimera - A visualization system for exploratory research and analysis. J. Comput. Chem. (2004), 1605−1612. https://doi.org/ 10.1002/jcc.20084.

[36] P. Santofimia-Castaño, B. Rizzuti, Á.L. Pey, P. Soubeyran, M. Vidal, R. Urrutia, J.L. Iovanna, J.L. Neira, Intrinsically disordered chromatin protein NUPR1 binds to the C-terminal region of Polycomb RING1B. PNAS (2017), 6332-6341. https://doi.org/ 10.1073/pnas.1619932114.

[37] R. Lappano, C. Mallet, B. Rizzuti, F. Grande, G.R. Galli, C. Byrne, I. Broutin, L. Boudieu, A. Eschalier, Y. Jacquot, M. Maggiolini, The Peptide ERα17p Is a GPER Inverse Agonist that Exerts Antiproliferative Effects in Breast Cancer Cells. Cells (2019), 590. https://doi.org/10.3390/cells8060590.

[38] M. Sugawara, J.M. Resende, C. Mendonca de Moraes, J.F. Chich, A. Marquette, M.H. Metz-Boutigue, B. Bechinger, Membrane structure and interactions of human Catestatin by multidimensional solution and solid-state NMR spectroscopy. FASEB J. (2010), 1737-1746. https://doi.org/ 10.1096/fj.09-142554.

760 [39] F. Grande, B. Rizzuti, M.A. Occhiuzzi, G. Ioele, T. Casacchia, F. Gelmini, R. Guzzi, A. Garofalo,
761 G. Statti, Identification by molecular docking of homoisoflavones from Leopoldia comosa as ligands
762 of estrogen receptors. Molecules (2018), 23, 894. https://doi.org/10.3390/molecules23040894.
763 [40] T. Casacchia, M.A. Occhiuzzi, F. Grande, B. Rizzuti, M.C. Granieri, C. Rocca, A. Gattuso, A.
764 Garofalo, T. Angelone, G. Statti, A pilot study on the nutraceutical properties of the Citrus hybrid
765 Tacle® a dietary source of polyphenols for supplementation in metabolic disorders. J. Funct. Foods
766 (2019), 370-381. https://doi.org/10.1016/j.jff.2018.11.030.
767 [41] T. Angelone, E. Filice, A.M. Quintieri, S. Imbrogno, N. Amodio, T. Pasqua, D. Pellegrino, F. Mulè,
768 M.C. Cerra, Receptor identification and physiological characterisation of glucagon-like peptide-2 in
769 the rat heart. Nutr. Metab. Cardiovasc. Dis. (2012), 486-94.
770 https://doi.org/10.1016/j.numecd.2010.07.014.
771 [42] I.C. Nettore, C. Rocca, G. Mancino, L. Albano, D. Amelio, F. Grande, F. Puoci, T. Pasqua, S.
772 Desiderio, R. Mazza, D. Terracciano, A. Colao, F. Bèguinot, G.L. Russo, M. Dentice, P.E. Macchia,
773 M.S. Sinicropi, T. Angelone, P. Ungaro, Quercetin and its derivative Q2 modulate chromatin
774 dynamics in adipogenesis and Q2 prevents obesity and metabolic disorders in rats. J. Nutr. Biochem.
775 (2019), 69:151-162. https://doi.org/10.1016/j.jnutbio.2019.03.019.
776 [43] Y. Wang, L. Su, M.D. Morin, B.T. Jones, L.R. Whitby, M.M.R.P. Surakattula, H. Huang, H. Shi,
777 J.H. Choi, K. Wang, E.M.Y. Moresco, M. Berger, X. Zhan, H. Zhang, D.L. Boger, B. Beutler,
778 TLR4/MD-2 activation by a synthetic agonist with no similarity to LPS. PNAS (2016), 884-893.
779 https://doi.org/10.1073/pnas.1525639113.
780 [44] Z. Golkar, O. Bagasra, D.G. Pace, Bacteriophage therapy: a potential solution for the antibiotic
781 resistance crisis. J. Infect. Dev. Ctries. (2014), 129-136. https://doi.org/10.3855/jidc.3573.
782 [45] M. Mahlapuu, J. Håkansson, L. Ringstad, C. Björn, Antimicrobial Peptides: An Emerging Category
783 of Therapeutic Agents. Front. Cell. Infect. Microbiol. (2016), 6, 194.
784 https://doi.org/10.3389/fcimb.2016.00194.
785 [46] R.E. Hancock, H.G. Sahl, Antimicrobial and host-defense peptides as new anti-infective therapeutic
786 strategies. Nat. Biotechnol. (2006), 1551–1557. https://doi.org/10.1038/nbt1267.
787 [47] M.R. Yeaman, N.Y. Yount, Mechanisms of antimicrobial peptide action and resistance. Pharmacol.
788 Rev. (2003), 27-55. https://doi.org/10.1124/pr.55.1.2.
789 [48] M.H. Metz-Boutigue, A.E. Kieffer, Y. Goumon, D. Aunis, Innate immunity: involvement of new
790 neuropeptides. Trends Microbiol. (2003), 585-92. https://doi.org/10.1016/j.tim.2003.10.001.
791 [49] Q. Su, J. Yao, C. Sheng, Geniposide Attenuates LPS-Induced Injury via Up-Regulation of miR-145
792 in H9c2 Cells. Inflammation (2018), 1229–1237. https://doi.org/10.1007/s10753-018-0769-8.
793 [50] R. Wang, D. Li, J. Ouyang, X. Tian, Y. Zhao, X. Peng, S. Li, G. Yu, J. Yang, Leonurine alleviates
794 LPS-induced myocarditis through suppressing the NF-κB signaling pathway. Toxicology (2019),
795 422:1-13. https://doi.org/ 10.1016/j.tox.2019.04.011.

[51] T.H. Htwe, N.M. Khardori, Cardiac emergencies: infective endocarditis, pericarditis, and myocarditis. Med. Clin. North Am. (2012), 1149-69. https://doi.org/ 10.1016/j.mcna.2012.09.003.

[52] R. Hao, G. Su, X. Sun, X. Kong, C. Zhu 2, G. Su, Adiponectin attenuates lipopolysaccharide-induced cell injury of H9c2 cells by regulating AMPK pathway. Acta Biochim Biophys Sin (Shanghai) (2019), 51(2):168-177. doi: 10.1093/abbs/gmy162.

[53] N.H. Evans, Chiral Catenanes and Rotaxanes: Fundamentals and Emerging Applications. Chemistry (2018), 3101-3112. https://doi.org/10.1002/chem.201704149.

[54] L. Chen, W. Fu, L. Zheng, Y. Wang, G. Liang, Recent progress in the discovery of myeloid differentiation 2 (MD2) modulators for inflammatory diseases. Drug Discov. today (2018), 1187-1202. https://doi.org/10.1016/j.drudis.2018.01.015.

[55] Y. Nagai, S. Akashi, M. Nagafuku, M. Ogata, Y. Iwakura, S. Akira, T. Kitamura, A. Kosugi, M. Kimoto, K. Miyake, Essential role of MD-2 in LPS responsiveness and TLR4 distribution. Nat. Immunol. (2002), 667-672. https://doi.org/ 10.1038/ni809.

[56] Y.C. Lu, W.C. Yeh, P.S. Ohashi, LPS/TLR4 signal transduction pathway. Cytokine (2008), 145-151. https://doi.org/ 10.1016/j.cyto.2008.01.006.

[57] J.L. Lai, Y.H. Liu, C. Liu, M.P. Qi, R.N. Liu, X.F. Zhu, Q.G. Zhou, Y.Y. Chen, A.Z. Guo, C.M. Hu, Indirubin Inhibits LPS-Induced Inflammation via TLR4 Abrogation Mediated by the NF-kB and MAPK Signaling Pathways. Inflammation (2017), (1):1-12. https://doi.org/10.1007/s10753-016-0447-7.

[58] Y.J. Choi, W.S. Lee, E.G. Lee, M.S. Sung, W.H. Yoo, Sulforaphane inhibits IL-1beta-induced proliferation of rheumatoid arthritis synovial fibroblasts and the production of MMPs, COX-2, and PGE2. Inflammation (2014), 1496-503. https://doi.org/10.1007/s10753-014-9875-4.

[59] B. Hoesel, J.A. Schmid, The complexity of NF-kappaB signaling in inflammation and cancer. Mol. Cancer (2013), 12, 86. https://doi.org/ 10.1186/1476-4598-12-86.

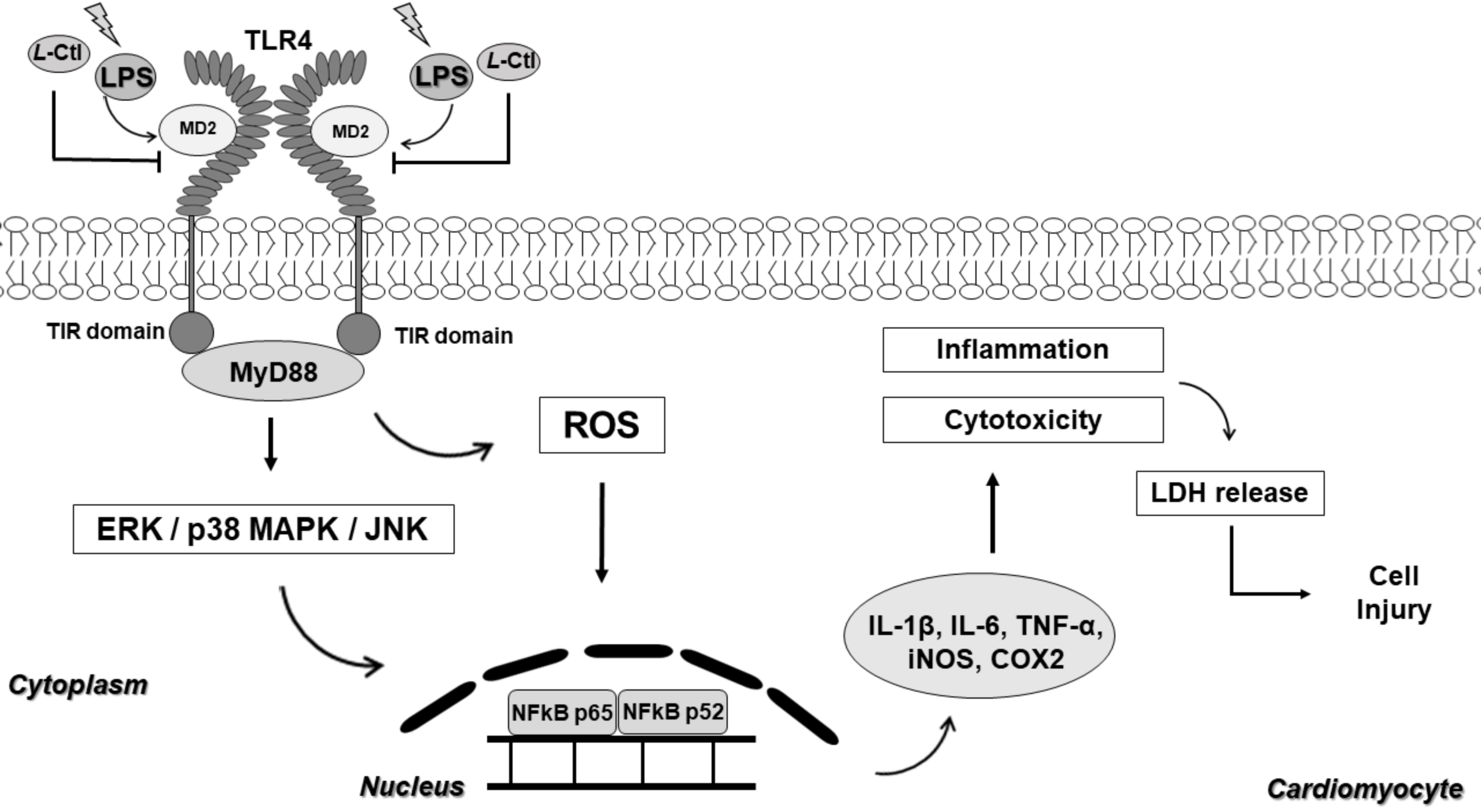
[60] A. Valaperti, Drugs targeting the canonical NF-κB pathway to treat viral and autoimmune myocarditis. Curr. Pharm. Des. (2016), 440–449. https://doi.org/10.2174/1381612822666151222160409.

[61] T. Yu, D. Dong, J. Guan, J. Sun, M. Guo, Q. Wang, Alprostadil attenuates LPS-induced cardiomyocyte injury by inhibiting the Wnt5a/JNK/NF-kappaB pathway. Herz (2020), (Suppl 1):130-138. https://doi.org/10.1007/s00059-019-4837-0.

[62] C. Huang, Y. Zhang, H. Qi, X. Xu, L. Yang, J. Wang, Myc is involved in Genistein protecting against LPS-induced myocarditis in vitro through mediating MAPK/JNK signaling pathway. Biosci Rep (2020), 40(6):BSR20194472. https://doi.org/10.1042/BSR20194472.

[63] R.M. Guo, W.M. Xu, J.C. Lin, L.Q. Mo, X.X Hua, P.X. Chen, K. Wu, D.D. Zheng, J.Q. Feng, Activation of the p38 MAPK/NF-κB pathway contributes to doxorubicin-induced inflammation and cytotoxicity in H9c2 cardiac cells. Mol. Med. Rep. (2013), 603-8. https://doi.org/10.3892/mmr.2013.1554.

833 [64] S.F. Liu, A.B. Malik, NF-kappa B activation as a pathological mechanism of septic shock and
834 inflammation. Am. J. Physiol. Lung Cell. Mol. Physiol. (2006), 622-645.
835 https://doi.org/10.1152/ajplung.00477.2005.
836 [65] F. Schneider, C. Marban, G. Ajob, S. Helle, M. Guillot, A. Launoy, Q. Maestraggi, F. Scavello, O.
837 Rohr, M.H. Metz-Boutigue, In Trauma Patients, the Occurrence of Early-Onset Nosocomial
838 Infections is Associated With Increased Plasma Concentrations of Chromogranin A. Shock (2018),
839 522-528. https://doi.org/10.1097/SHK.0000000000001000
840 [66] Y.C. Tien, J.Y. Lin, C.H. Lai, C.H. Kuo, W.Y. Lin, C.H. Tsai, F.J. Tsai, Y.C. Cheng, W.H. Peng,
841 C.Y. Huang, Carthamus tinctorius L. prevents LPS-induced TNFalpha signaling activation and cell
842 apoptosis through JNK1/2-NFkappaB pathway inhibition in H9c2 cardiomyoblast cells. J.
843 Ethnopharmacol. (2010), 505-13. https://doi.org/10.1016/j.jep.2010.05.038
844 [67] H. Yuan, C.N. Perry, C. Huang, E. Iwai-Kanai, R.S. Carreira, C.C. Glembotski, R.A. Gottlieb, LPS-
845 induced autophagy is mediated by oxidative signaling in cardiomyocytes and is associated with
846 cytoprotection. Am. J. Physiol. Heart Circ. Physiol. (2009), 470-9.
847 https://doi.org/10.1152/ajpheart.01051.2008.
848 [68] S. Lei, Y. Zhang, W. Su, L. Zhou, J. Xu, Z.Y. Xia, Remifentanil attenuates lipopolysaccharide-
849 induced oxidative injury by downregulating PKCβ2 activation and inhibiting autophagy in H9C2
850 cardiomyocytes. Life Sci. (2018),109-115. https://doi.org/10.1016/j.lfs.2018.10.041.
851 [69] W.L. DeLano, The PyMOL molecular graphics system. DeLano Scientific, Palo Alto, (2002).


L-Ctl
LPS
TLR4
LPS
L-Ctl
MD2
MD2
TIR domain
TIR domain
MyD88
ROS
ERK / p38 MAPK / JNK
Inflammation
Cytotoxicity
LDH release
Cell Injury
IL-1β, IL-6, TNF-α, iNOS, COX2
NFkB p65
NFkB p52
Cytoplasm
Nucleus
Cardiomyocyte